

This work was written as part of one of the author's official duties as an Employee of the United States Government and is therefore a work of the United States Government. In accordance with 17 U.S.C. 105, no copyright protection is available for such works under U.S. Law.

Public Domain Mark 1.0

<https://creativecommons.org/publicdomain/mark/1.0/>

Access to this work was provided by the University of Maryland, Baltimore County (UMBC) ScholarWorks@UMBC digital repository on the Maryland Shared Open Access (MD-SOAR) platform.

**Please provide feedback**

Please support the ScholarWorks@UMBC repository by emailing [scholarworks-group@umbc.edu](mailto:scholarworks-group@umbc.edu) and telling us what having access to this work means to you and why it's important to you. Thank you.

# Whistler propagation and modulation in the presence of nonlinear Alfvén waves

R. P. Sharma,<sup>1</sup> M. L. Goldstein,<sup>2</sup> Navin Kumar Dwivedi,<sup>1</sup> and Prashant K. Chauhan<sup>3</sup>

Received 20 November 2009; revised 8 July 2010; accepted 24 August 2010; published 4 December 2010.

[1] This paper presents the modulation of whistler waves due to linear interactions between a weak whistler signal and a pump kinetic Alfvén wave (KAW) in intermediate- $\beta$  ( $m_e/m_i \ll \beta \ll 1$ ) plasmas (where  $\beta$  is the ratio of the ion sound speed to the Alfvén speed). As a consequence of ponderomotive nonlinearity, the pump KAW becomes filamented when its power exceeds the threshold for the filamentation instability. The periodic enhancements of the whistler amplitude occur in the locations where the beam width is narrower and are thus produced by the focusing of the whistler beam. Our results reveal that KAW has a (magnetic) power spectrum with an approximate scaling of  $k^{-5/3}$  (where  $k$  is  $|k|$ ). The amplified whistler has electric field power spectra that are steeper than  $k^{-8/3}$  (where  $k$  is  $|k|$ ). These results are consistent with recent observations by the Cluster spacecraft in the magnetotail region of the Earth's magnetosphere.

**Citation:** Sharma, R. P., M. L. Goldstein, N. K. Dwivedi, and P. K. Chauhan (2010), Whistler propagation and modulation in the presence of nonlinear Alfvén waves, *J. Geophys. Res.*, 115, A12207, doi:10.1029/2009JA015123.

## 1. Introduction

[2] Alfvén waves are commonly observed in space plasmas, especially in the solar wind [Coleman, 1966; Unti and Neugebauer, 1968; Belcher and Davis, 1971], the magnetosheath [Sahraoui et al., 2003], the auroral regions [Norqvist et al., 1996; Stasiewicz et al., 2000a], and throughout the solar system [Wygant et al., 2002; Stasiewicz et al., 2000b]. At small scales, when the wave vectors are transverse to the background magnetic field, these waves are known as kinetic Alfvén waves (KAWs) [Stefant, 1970] and may accelerate ions and electrons [Goertz and Boswell, 1979; Chen et al., 2001]. These waves play an important role in coronal heating, the acceleration of solar wind [Cranmer et al., 1999], and the dissipation of solar wind turbulence [Leamon et al., 2000; Sahraoui et al., 2009]. Alfvén waves may play a key role in driving magnetic reconnection, and some observations indicate that KAWs may play an important role in facilitating magnetic reconnection [Chaston et al., 2009]. However, some studies [Rogers et al., 2001] suggest that fast reconnection in collisionless systems depends on the dynamics of whistler waves and/or KAWs at small scales. The generation of an Alfvén wave by mixing of two whistler waves has been studied by Larsson and Stenflo [1975].

[3] Whistler is an extraordinary mode of electromagnetic wave propagation in magnetized plasmas. There are

many physical phenomena in which one encounters whistler wave turbulence; examples include turbulence excited by energetic particles in the radiation belts of Earth's magnetosphere [Kennel and Engelmann, 1966] and waves excited in the magnetic field reconnection region in Earth's magnetotail.

[4] Recent laboratory experiments show a positive correlation between the reconnection rate and the magnitude of electromagnetic fluctuations up to the lower hybrid frequency [Ji et al., 2004]. From an analysis of data from the four Cluster spacecraft, Eastwood et al. [2009] presented, for the first time, the spectral properties of both the electric and magnetic field fluctuations in an ion diffusion region. They used these spectra to determine the nature of the waves in the dissipation range, specifically whether energy is deposited in the form of KAWs [Leamon et al., 1999] or whistler waves [Stawicki et al., 2001].

[5] Nonlinear whistler wave scattering by KAW can play an important role in exchanging energy between very-low-frequency and ultra-low-frequency radiation in space plasmas, for example, in the magnetosphere of Earth. The nonlinear scattering of whistler waves by KAWs [Yukhimuk et al., 1999] is thought to be a possible mechanism for enhancing and generating geomagnetic pulsations in Earth's magnetosphere and ionosphere.

[6] Simulation work carried out by Gary et al. [2008] demonstrates that whistler turbulence can significantly contribute to the relatively steep high-frequency power law spectra observed in solar wind, which they call the “dispersion range.” However, their work does not resolve the controversy of whether these spectra are due to whistler or kinetic Alfvén fluctuations; in general, it is possible for both modes to be present, with their relative contributions varying as plasma conditions change.

<sup>1</sup>Centre for Energy Studies, Indian Institute of Technology, Delhi, India.

<sup>2</sup>NASA Goddard Space Flight Center, Greenbelt, Maryland, USA.

<sup>3</sup>Grupo de Laser e Plasmas, Instituto Superior Técnico, Lisbon, Portugal.

[7] Therefore, there are various situations (such as in magnetic reconnection or solar wind turbulence at higher frequency side) where the pertinent question is whether the energy is in the form of KAW or whistler or both. To understand, we propose the following model. The essence of this model is that as a consequence of ponderomotive nonlinearity, the pump KAW gets filamented. The evolution of whistler spectrum is caused by the linear whistler propagation and refraction in the stationary plasma inhomogeneities produced by KAW.

[8] In this paper, we first study the filamentary structures of KAWs in an intermediate- $\beta$  plasma. The linear interaction of a weak whistler signal propagating in these filamentary structures has been studied. The formation of KAW filamentary structures has been studied semi-analytically when the KAW has a Gaussian intensity distribution along  $x$  under a paraxial approximation. The linear propagation of the weak whistler wave in the modified nonlinear plasma density filaments produced by the KAW has been studied. The KAW and whistler system of equations are used to obtain the KAW and whistler structures along the direction of propagation. These data are used further to obtain the anisotropy and power spectra of the KAW and whistler fluctuations using parameters relevant to the magnetotail region of Earth's magnetosphere. The relevance of these studies to anisotropy [Schekochihin et al., 2009; Cho and Lazarian, 2004, 2009] and power spectra (as observed by Cluster spacecraft in the magnetotail region) is also pointed out.

[9] The organization of this paper is as follows: the brief summary of model equations and numerical results appropriate for KAW in the intermediate- $\beta$  plasmas, and its interaction with weak whistler signal, are given in sections 2 and 3, respectively. Section 4 comprises the conclusions.

## 2. Model Equations of KAW

[10] Let us consider the propagation (in the  $x$ - $z$  plane) of a low-frequency, finite amplitude KAW in the magnetized plasma having ambient magnetic field  $B_0$  along the  $z$ -axis. Using the drift approximation, Maxwell's equations, and following the standard method [Bellan and Stasiewicz, 1998; Shukla and Sharma, 2002; Shukla and Stenflo, 1999, 2000; Shukla et al., 1999], the dynamical equation governing the propagation of the KAW can be obtained as follows:

$$\frac{\partial^2 B_y}{\partial t^2} = -(V_{Te}^2 \lambda_e^2 + V_A^2 \rho_i^2) \frac{\partial^4 B_y}{\partial x^2 \partial z^2} + V_A^2 \frac{\partial^2 B_y}{\partial z^2} - V_A^2 \frac{\partial}{\partial z} \left( \frac{\delta n_s}{n_0} \frac{\partial B_y}{\partial z} \right), \quad (1)$$

where  $\delta n_s = n_e - n_0$  is the number density change, with  $n_e$  being the modified electron density and  $n_0$  being the electron density of plasma in the absence of waves,  $V_{Te} (= \sqrt{T_e/m_e})$  being the electron thermal speed,  $T_e$  ( $T_i$ ) being the electron (ion) temperature,  $m_e$  ( $m_i$ ) being the mass of the electron (ion),  $\lambda_e (= \sqrt{c^2 m_e / 4\pi n_0 e^2})$  being the collisionless electron skin depth,  $V_A (= \sqrt{B_0^2 / 4\pi n_0 m_i})$  being the Alfvén velocity,  $\rho_i (= V_{Ti} / \omega_{ci})$  being the ion gyroradius,  $V_{Ti} (= \sqrt{T_i / m_i})$  being the ion thermal speed, and  $\omega_0$  being the frequency of the

pump kinetic Alfvén wave. Here the density can be modified by the ponderomotive force of the KAW in intermediate- $\beta$  plasmas [Shukla and Stenflo, 2000] and is given as follows:

$$\frac{\delta n_s}{n_0} = \phi(\tilde{B}\tilde{B}), \quad (2)$$

where  $\phi(\tilde{B}\tilde{B}) = \exp(\gamma \tilde{B}\tilde{B}) - 1$ ,  $\gamma = [(1 - \alpha_0(1 + \delta)) / 16\pi n_0 T] (V_A^2 k_{0z}^2 / \omega_0^2)$ ,  $\alpha_0 = \omega_0^2 / \omega_{ci}^2$ ,  $\delta = m_e k_{0x}^2 / m_i k_{0z}^2$ , and  $\omega_{ci} (= eB_0 / m_i c)$  is the ion gyrofrequency,  $k_{0x}$  ( $k_{0z}$ ) is the component of the wave vector perpendicular (parallel) to  $\hat{z}B_0$ .

[11] The semi-analytical solution of equation (1) in two dimensions is obtained within the paraxial approximation ( $x \ll r_0 f_0$ ) by using the method developed by Akhmanov et al. [1968]; here  $r_0$  is the transverse scale size of the pump KAW, and  $f_0$  is the dimensionless beam width parameter given by equation (6). For this, first we consider a plane wave solution in steady state:

$$B_y = \tilde{B}_0(x, z) e^{i(k_{0x}x + k_{0z}z - \omega t)}. \quad (3)$$

[12] Using equation (3) in equation (1) and assuming  $\partial_z \tilde{B}_0 \ll k_{0z} \tilde{B}_0$  and  $\partial_x \tilde{B}_0 \gg k_{0x} \tilde{B}_0$ , we get the following:

$$-2ik_{0z} \frac{\partial \tilde{B}_0}{\partial z} - \frac{k_{0z}^2}{V_A^2} (V_{Te}^2 \lambda_e^2 + V_A^2 \rho_i^2) \frac{\partial^2 \tilde{B}_0}{\partial x^2} - k_{0z}^2 \phi(\tilde{B}_0 \tilde{B}_0^*) \tilde{B}_0 = 0. \quad (4)$$

[13] The solution for  $\tilde{B}_0$  can be written as follows:

$$\begin{aligned} \tilde{B}_0 &= \tilde{A}_0 \exp(ik_{0z}S_0(x, z)) \\ \tilde{A}_0^2 &= \frac{\tilde{B}_{00}^2}{f_0} \exp\left(\frac{-x^2}{r_0^2 f_0^2}\right) \\ S_0 &= \zeta \frac{x^2}{2} + \phi_0 \\ \zeta &= a \frac{1}{f_0} \frac{df_0}{dz} \end{aligned} \quad (5)$$

where in equation (5),  $a = \{(\rho_i^2 + \rho_s^2)k_{0z}^2\}^{-1}$ ,  $\rho_s (= c_s / \omega_{ci})$  is the ion gyroradius at electron temperature,  $c_s (= \sqrt{T_e / m_i})$  is the ion sound speed, and  $f_0$  is the dimensionless beam width parameter governed by the differential equation

$$\frac{d^2 f_0}{dz^2} = \frac{1}{a^2 R_d^2 f_0^3} - \frac{\gamma \tilde{B}_{00}^2}{a r_0^2 f_0^2} \exp\left(\frac{\gamma \tilde{B}_0^2}{f_0^2}\right), \quad (6)$$

where  $R_d = k_{0z} r_0^2$ .

[14] On the right-hand side of equation (6), the first term accounts for the diffraction of the KAW because of its finite transverse size, while the second term accounts for the nonlinearity. The field of the main KAW is governed by these diffraction and nonlinear terms. A self-trapping mode is obtained when the two terms on the right-hand side of equation (6) balance. The wave then propagates without convergence or divergence (viz.,  $f_0 = 1$ ). In this case, the critical magnetic field  $\tilde{B}_{00(cr)}$  can be obtained by balancing the two terms on the right-hand side of equation (6).

[15] To get the parameter values to be used in the simulation, we use the plasma parameters typical of the

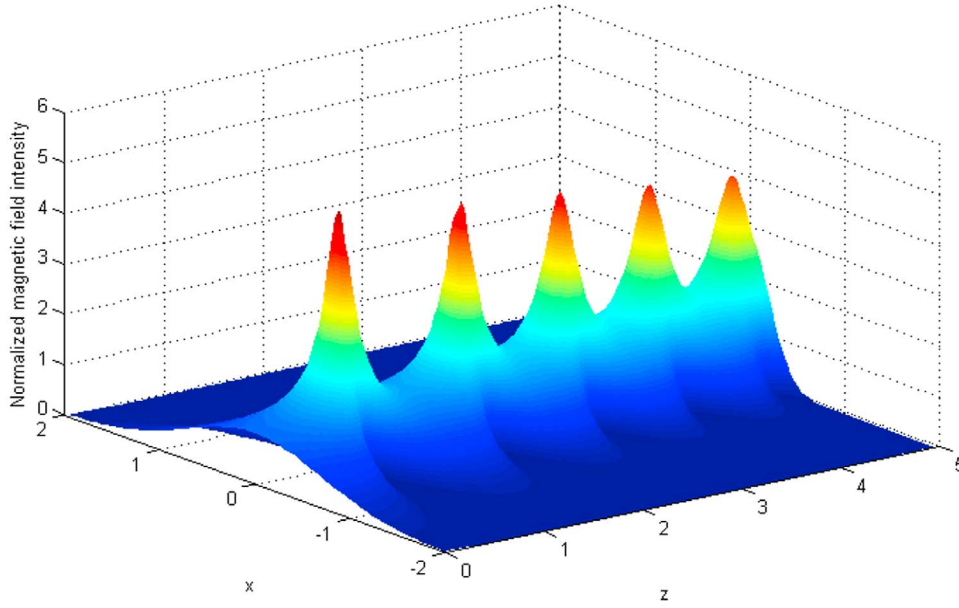


**Figure 1.** The variation of magnetic field intensity (normalized by  $\tilde{B}_{00}^2$ ) of kinetic Alfvén wave (KAW) with  $x$  and normalized distance of propagation,  $\xi = z/R_d$  (denoted by  $z$ ).

Earth's magnetotail:  $B_0 = 20 \times 10^{-5}$  G,  $n_0 = 0.05$  cm $^{-3}$ ,  $T_e = 5 \times 10^3$  K,  $T_i = 5 \times 10^7$  K and  $\beta = 0.2$ . Using these values, one finds that  $\omega_{ci} = 1.92$  Hz,  $\lambda_e = 2.38 \times 10^6$  cm,  $V_A = 1.95 \times 10^8$  cm s $^{-1}$ ,  $V_{Te} = 2.75 \times 10^7$  cm s $^{-1}$ ,  $V_{Ti} = 6.43 \times 10^7$  cm s $^{-1}$ ,  $\rho_i = 3.36 \times 10^7$  cm,  $\rho_s = 3.35 \times 10^5$  cm,  $a = 9.33 \times 10^3$ , and  $r_0 = 7.3 \times 10^7$  cm. For  $\omega_0 = 0.06$  Hz and  $k_{0x}\rho_s = 0.001$ , one gets  $k_{0z} = 3.07 \times 10^{-10}$  cm $^{-1}$ , and  $k_{0x} = 2.99 \times 10^{-9}$  cm $^{-1}$ . For these parameters, the critical value of KAW field  $\tilde{B}_{00(cr)}$  comes out to be  $6.08 \times 10^{-7}$  G. If the initial value of the KAW field is more than this value, then the beam will focus and its width can be obtained from equation (6).

[16] We solved equation (6) for the KAW beam width  $f_0$  with the initial conditions for the plane wave front as  $df_0/dz = 0$  and  $f_0 = 1$  at  $z = 0$ .

[17] The other parameter values are the initial KAW field  $\tilde{B}_{00} = 4.04 \times 10^{-5}$  G,  $R_d = 1.63 \times 10^6$  cm, and  $\gamma = 5.77 \times 10^{11}$ .

[18] Figure 1 depicts the magnetic intensity (normalized by  $\tilde{B}_{00}^2$ ) distribution of the main KAW, with  $x$  and normalized distance of propagation,  $\xi = z/R_d$  (denoted by  $z$  in Figure 1) in the magnetotail region. As shown in the figure, filamentary structures are at different locations. This can be explained from equation (6). When the initial magnetic field of the main KAW is more than its critical magnetic field, the nonlinear term (second term on the right-hand side of equation (6)) dominates and the value of  $f_0$  decreases with the distance of propagation. But when  $f_0$  becomes very small, the diffraction term (first term on the right-hand side of equation (6)) starts dominating. Therefore,  $f_0$  increases with the distance of the propagation until  $f_0$  becomes so large that the diffraction term becomes smaller in comparison to the nonlinear term. Owing to the nonlinear effects,  $f_0$  further decreases until it becomes so small that the diffraction term again dominates and  $f_0$  starts diverging and this process repeats. Hence, the main KAW attains a certain minimum beam width  $f_0$ , and the intensity

of the main KAW in these small-size structures becomes very high.

[19] We studied the power spectrum of the field at  $x = 0$ . We show this in Figure 2 where  $|B_k|^2$  against  $k$  (where  $k$  is  $|k|$ ) is presented. In the figure, Kolmogorov  $k^{-5/3}$  scaling is also given for the sake of reference. The high-intensity filaments can induce other decaying waves and/

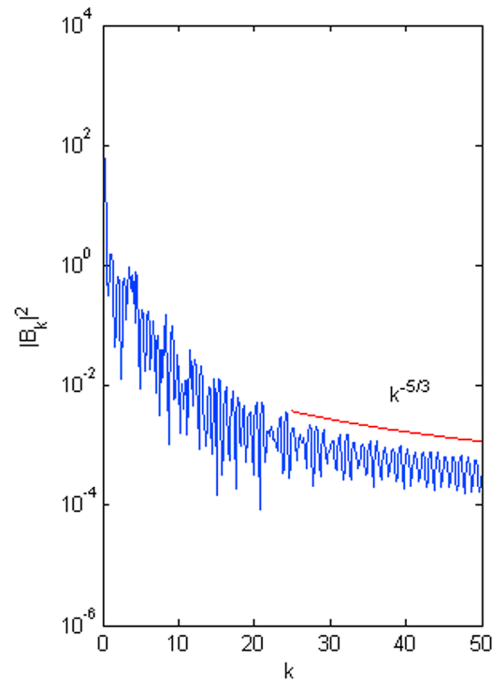


**Figure 2.** Normalized  $|B_k|^2$  against  $k$  (where  $k$  is  $|k|$ ) at  $x = 0$  of the KAW, and its normalization constant is  $R_d^{-1}$ .

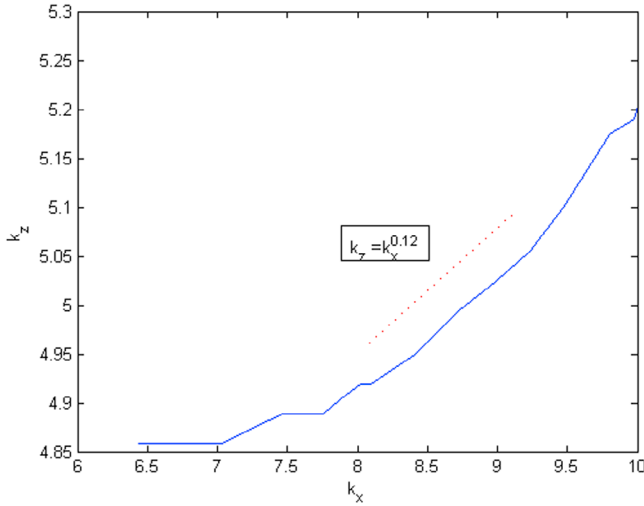


**Figure 3.** Anisotropy scaling of KAW by the present work.

or can become a source of further collapse of the KAWs, which will change the spectrum of the KAW and the spectral index. Goldstein *et al.* [1999] solved the MHD equations in spherical geometry and computed the power spectra. They found that for latter times and larger distances, the spectral index approached a value of  $-5/3$ . The wave number spectrum with a typical  $k^{-5/3}$  Kolmogorov form indicates quasi-steady spectral transfer and strong nonlinear couplings. So, the inferred power spectrum of magnetic field fluctuations indicates that the nonlinear interactions may be distributing energy among large and intermediate wave numbers.

[20] KAWs are highly anisotropic, with the perpendicular wavelengths being much shorter than the parallel ones ( $k_x \gg k_z$ ), and they exhibit significantly different dynamics along and across the background magnetic field. The anisotropic behavior of KAW is shown in Figure 3. It is clear from Figure 3 that KAW has anisotropy of  $k_z \propto k_x^{0.12}$  in the present simulation. Schekochihin *et al.* [2009] estimated the anisotropic scaling of KAW as  $k_z \propto k_x^{1/3}$  on the basis of heuristic arguments. Cho and Lazarian [2004, 2009] have given the anisotropic scaling in the case of electron magnetohydrodynamic (EMHD) simulations by taking a particular choice of filtering wave numbers. Their scaling was  $k_z \propto k_x^{1/3}$ , but they reported that the scaling was weaker if the choice of the filtering wave numbers was changed. In our model, the deviation in anisotropic scaling from the literature [Schekochihin *et al.*, 2009; Cho and Lazarian, 2004, 2009] may be due to the paraxial method which we are using here and the limitation of the choice of the filtering wave numbers as mentioned by [Cho and Lazarian, 2004, 2009].

[21] In the present work we have studied a nonlinear self-focusing and filamentation of the KAW. A weak whistler signal propagating in the density filaments produced by the KAW self-focusing gets modulated, which leads to the periodic enhancements of the whistler amplitude at the places where the beam width is narrower. To model this, we have developed the two nonlinear equations

as given in the next section, where the whistler waves are assumed to be propagating along the magnetic field lines.

### 3. Model Equations of Whistler

[22] Let us consider the propagation of whistler waves along the magnetic field lines ( $z$ -direction). The wave equation in its general form for a field varying as  $e^{-i\omega t}$  is written as follows:

$$\nabla^2 \vec{E} - \nabla(\nabla \cdot \vec{E}) = -\frac{\omega^2}{c^2} \bar{\epsilon} \cdot \vec{E}. \quad (7)$$

[23] Here  $\bar{\epsilon}$  is the dielectric tensor. The wave equations in component form are as follows:

$$\frac{\partial^2 E_x}{\partial z^2} - \frac{\partial}{\partial x} \frac{\partial E_z}{\partial z} = -\frac{\omega^2}{c^2} (\bar{\epsilon} \cdot \vec{E})_x. \quad (8)$$

$$\frac{\partial^2 E_y}{\partial z^2} + \frac{\partial^2 E_y}{\partial x^2} = -\frac{\omega^2}{c^2} (\bar{\epsilon} \cdot \vec{E})_y. \quad (9)$$

[24] Let the two coupled modes be denoted as  $A_1$  and  $A_2$ ; one is right circularly polarized and the other is left circularly polarized and defined as follows:

$$A_1 = E_x + iE_y, \quad (10)$$

and

$$A_2 = E_x - iE_y. \quad (11)$$

[25] From equations (8) and (9) and taking  $\partial/\partial y = 0$ , one can get

$$\frac{\partial^2 A_1}{\partial z^2} + \frac{1}{2} \left( 1 + \frac{\epsilon_{+00}}{\epsilon_{00}} \right) \frac{\partial^2 A_1}{\partial x^2} + \frac{1}{2} \left( -1 + \frac{\epsilon_{-00}}{\epsilon_{00}} \right) \frac{\partial^2 A_2}{\partial x^2} + \frac{\omega^2}{c^2} \epsilon_{+0} A_1 = 0, \quad (12)$$

and

$$\frac{\partial^2 A_2}{\partial z^2} + \frac{1}{2} \left( 1 + \frac{\epsilon_{-00}}{\epsilon_{00}} \right) \frac{\partial^2 A_2}{\partial x^2} + \frac{1}{2} \left( -1 + \frac{\epsilon_{+00}}{\epsilon_{00}} \right) \frac{\partial^2 A_1}{\partial x^2} + \frac{\omega^2}{c^2} \epsilon_{-0} A_2 = 0. \quad (13)$$

[26] On assuming  $A_1 = 0$ , equation (13) for  $A_2$  gives the following:

$$\frac{\partial^2 A_2}{\partial z^2} + \frac{1}{2} \left( 1 + \frac{\epsilon_{-00}}{\epsilon_{00}} \right) \frac{\partial^2 A_2}{\partial x^2} + \frac{\omega^2}{c^2} \epsilon_{-0} A_2 = 0, \quad (14)$$

where  $\epsilon_0 = 1 - \omega_p^2 \left( 1 + \frac{\delta n_s}{n_0} \right) / \omega^2$ ,  $\epsilon_{+0} = 1 - \omega_p^2 \left( 1 + \frac{\delta n_s}{n_0} \right) / \omega(\omega + \omega_{ce})$ ,  $\epsilon_{-0} = 1 - \omega_p^2 \left( 1 + \frac{\delta n_s}{n_0} \right) / \omega(\omega - \omega_{ce})$ ,  $\epsilon_{-00}$  is

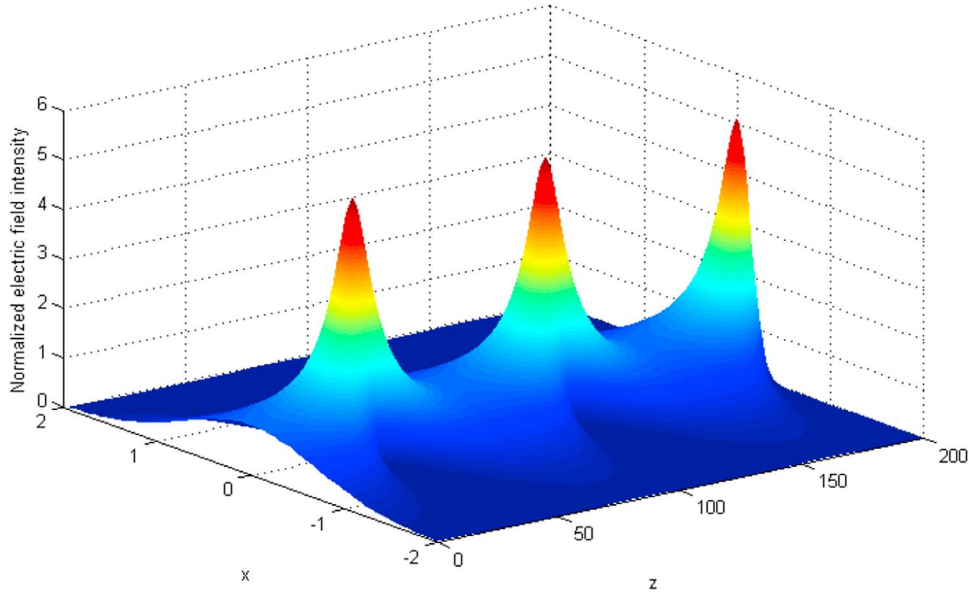


**Figure 4.** The variation of electric field intensity (normalized by  $E_{00}^2$ ) of the whistler wave with  $x$  and normalized distance of propagation,  $\xi = z/R_d$  (denoted by  $z$ ).

the linear part of  $\varepsilon_{-0}$  and  $\varepsilon_{00}$  is the linear part of  $\varepsilon_0$ , and

$\omega_p (= \sqrt{4\pi n_0 e^2 / m_e})$  is the electron plasma frequency,  $\omega_{ce}$  ( $= eB_0 / m_e c$ ) is the electron gyrofrequency,  $\omega$  is the whistler wave frequency, and  $\delta n_s = n_e - n_0$  (given by equation (2)).

[27] To obtain the solution of equation (14), we consider a generalized plane wave solution

$$A_2 = A e^{-i(\omega t - k_- z)}, \quad (15)$$

where  $k_- = \omega \varepsilon_{-00}^{1/2} / c$ ,  $\varepsilon_{-00}$  is the linear part of  $\varepsilon_{-0}$  and  $A$  is the complex amplitude.

[28] On substituting this solution in equation (14) and assuming  $\partial_z A \ll k_- A$ , we get

$$-2ik_- \frac{\partial A}{\partial z} + \frac{1}{2} \left( 1 + \frac{\varepsilon_{-00}}{\varepsilon_{00}} \right) \frac{\partial^2 A}{\partial x^2} + \frac{\omega^2}{c^2} \varepsilon_{-0} A - k_-^2 A = 0. \quad (16)$$

[29] Equation (16) can be written for real and imaginary parts separately by introducing the additional eikonal, i.e.,  $A = A_0(x) e^{ik_- S(x)}$ .

[30] The real part is

$$2 \frac{\partial S}{\partial z} + \frac{1}{2} \left( 1 + \frac{\varepsilon_{-00}}{\varepsilon_{00}} \right) \left( \frac{\partial S}{\partial x} \right)^2 = \frac{1}{2k_-^2 A_0} \left( 1 + \frac{\varepsilon_{-00}}{\varepsilon_{00}} \right) \frac{\partial^2 A_0}{\partial x^2} \varepsilon_{-0}, \quad (17)$$

and the imaginary part is

$$\frac{\partial A_0^2}{\partial z} + \frac{1}{2} A_0^2 \left( 1 + \frac{\varepsilon_{-00}}{\varepsilon_{00}} \right) \frac{\partial^2 S}{\partial x^2} + \frac{1}{2} \left( 1 + \frac{\varepsilon_{-00}}{\varepsilon_{00}} \right) \frac{\partial S}{\partial x} \frac{\partial A_0^2}{\partial x} = 0. \quad (18)$$

[31] Solutions of equations (17) and (18) can be written as follows:

$$A_0^2 = \frac{E_{00}^2}{f_-} e^{-x^2 / r_d^2 f_-^2}, \quad (19)$$

$$S_- = \frac{x^2}{2} \varsigma(z) + \chi(z), \quad (20)$$

where

$$\varsigma(z) = \frac{1}{f_-(z)} \frac{df_-(z)}{dz} \frac{2}{\left( 1 + \frac{\varepsilon_{-00}}{\varepsilon_{00}} \right)}. \quad (21)$$

[32] Using equations (19)–(21) in equation (18), the equation for beam width parameter  $f_-$  for whistler waves

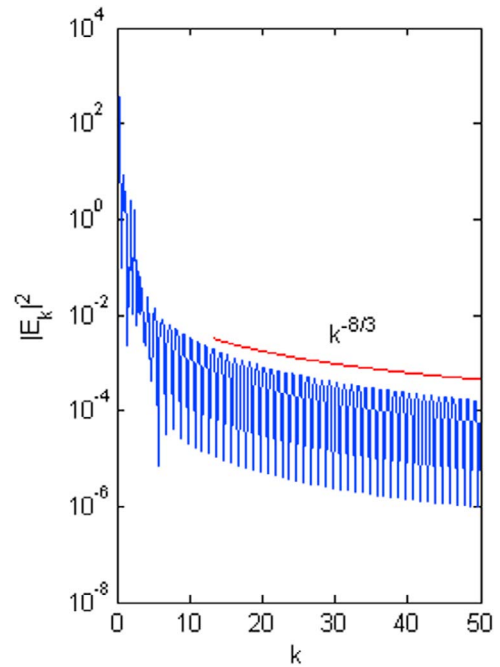


**Figure 5.** Normalized  $|E_k|^2$  against  $k$  (where  $k$  is  $|k|$ ) at  $x = 0$  of the whistler wave, and its normalization constant is  $R_{d1}^{-1}$ .



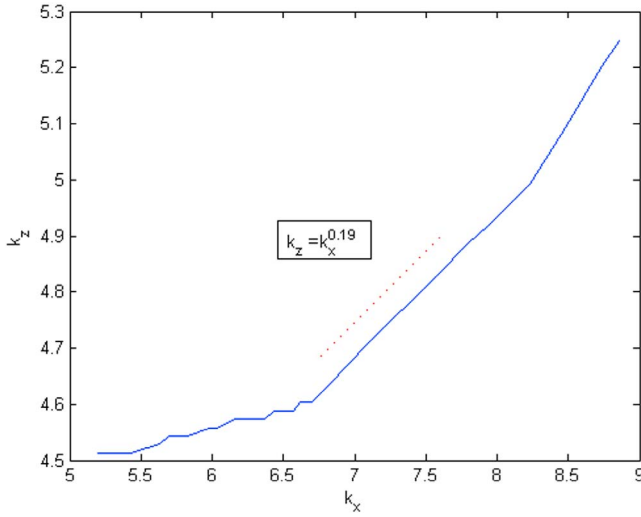


**Figure 6.** Anisotropy scaling of whistler wave by the present work.

can be obtained by equating the coefficient of  $x^2$  on both sides as follows:

$$\frac{d^2 f_-(z)}{dz^2} = \frac{1}{4} \frac{r_0^4}{R_{d1}^2 r_w^4} \left( 1 + \frac{\varepsilon_{-00}}{\varepsilon_{00}} \right) \frac{1}{f_-^3} - \frac{f_-}{2} \left( 1 + \frac{\varepsilon_{-00}}{\varepsilon_{00}} \right) \frac{\gamma B_{00}^2}{r_0^2 f_0^4} e^{\frac{\gamma B_{00}^2}{r_0^2}}. \quad (22)$$

where  $R_{d1} = k_- r_w^2$ . Now, we have solved equation (22) satisfied by the whistler beam width  $f_-$  with the initial conditions for  $f_-$  as the plane wave front, i.e.,  $df_-/dz = 0$  and  $f_- = 1$  at  $z = 0$ .

[33] The parameter values for the whistler wave used in the simulation are  $r_w = 7.3 \times 10^8$  cm,  $\omega = 76.64$  Hz,  $\omega_p = 1.26 \times 10^4$  Hz,  $k_- = 6.013 \times 10^{-8}$  cm $^{-1}$ , and  $R_{d1} = 3.20 \times 10^{10}$  cm.

[34] It is obvious from equation (22) that the value of  $f_-$  is governed by the competition of the diffraction term (first term on the right-hand side) and the nonlinear term (second term on the right-hand side). If there is no nonlinear term (when second term in equation (22) is zero), then the whistler wave would be continuously diverging and its intensity would decrease as given by equation (19). On the other hand, if the second term is finite (in equation (22)) and its magnitude is equal to the first term, then the whistler wave propagates without convergence and divergence ( $f_- = 1$ ). This means the whistler signal remains at constant amplitude as given by equation (19). To explain the whistler beam modifications caused by the linear beam propagation and refraction in the inhomogeneous plasma, we have solved equation (22) numerically for the parameters typical for KAW and whistler waves in the magnetotail region, as mentioned earlier in section 2.

[35] Figure 4 shows the variation of electric field intensity (normalized by  $E_{00}^2$ ) of the whistler wave with  $x$  and normalized distance of propagation,  $\xi = z/R_d$  (denoted by  $z$  in Figure 4). The filamentary structures of the whistler wave as observed in Figure 4 can be explained using equation (22). Initially, when the KAW becomes filamented, it modifies the electron density and creates the density dips. Because

the effective dielectric constant  $\varepsilon_{-0}$  of the whistler wave also depends upon the field intensity of the KAW, the second term in equation (22) becomes nonlinear. The whistler wave propagates through the modified nonlinear plasma density filaments produced by the KAW self-focusing, which leads to the periodic enhancements of the whistler amplitudes at the places where the beam width is narrower. The magnetic field intensity profile of the whistler wave as shown in Figure 4 is due to the combined effect of both diffraction term and nonlinear term. This interaction between KAW and whistler wave is so strong that the whistler wave becomes highly localized and acquires the maximum intensity at those positions where its beam width parameter  $f_-$  is minimum.

[36] We next studied the electric field power spectra of the whistler wave. Figure 5 shows the variation of  $|E_k|^2$  against  $k$  (where  $k$  is  $|k|$ ) at  $x = 0$ . The scaling  $k^{-8/3}$  is also shown as a reference. This type of scaling for the power spectra of whistler waves has been observed [Eastwood et al., 2009] recently by Cluster spacecraft within the magnetic reconnection ion diffusion region of the magnetotail. We also studied the anisotropic scaling of whistler wave. Figure 6 shows the anisotropic behavior of whistler wave; our simulation results reveal that whistler wave has anisotropic scaling of  $k_z \propto k_x^{0.19}$ .

#### 4. Conclusions

[37] In the present paper, we have studied the modulation of whistler wave due to linear interactions between a weak whistler signal and a pump KAW in intermediate- $\beta$  plasmas. Because of the ponderomotive nonlinearity of the pump KAW, the background electron density gets modified and the KAW is filamented. A weak whistler signal propagating in the modified nonlinear plasma density filaments produced by the KAW self-focusing gets modulated, which leads to the periodic enhancements of the whistler amplitudes at the places where the beam width is narrower. We have obtained the magnetic field intensity profile of the whistler wave. The results of this paper show that KAW has anisotropy of  $k_z \propto k_x^{0.12}$  and (magnetic) power spectra with the approximate scaling  $k^{-5/3}$ . The amplified (excited) whistler wave has anisotropy of  $k_z \propto k_x^{0.19}$ , and the electric field power spectrum is steeper than  $k^{-8/3}$ . These power spectra are consistent with the recent observations by the Cluster spacecraft in the magnetotail region of the Earth's magnetosphere [Eastwood et al., 2009], where whistler electric field power spectra steeper than  $k^{-8/3}$  have been observed. There are various situations, for example, in magnetic reconnection in the Earth's magnetotail region or in solar wind turbulence at high frequencies, where the pertinent question is whether the energy is in the form of KAW or whistler or both. The present paper shows that the energy is not in whistler waves but is in the KAW. Therefore, the present model will help in understanding these complex issues.

[38] It is worthwhile to mention here that in the present model, we are considering the self-focusing of the KAW as a nonlinear mechanism. But self-focusing is not a unique nonlinear process associated with KAW; some other nonlinear processes have been investigated that can compete with it. In particular, three-wave decay [Voitenko, 1998] and

generation of convective cells by kinetic Alfvén waves in the upper ionosphere (convective cell growth time is comparable to the parametric decay growth time ( $T_{\text{dnl}}$ ) [Onishchenko et al., 2004]) are often most efficient nonlinear processes for KAWs. These processes can spread out the initial KAW spectrum before the KAW self-focusing is developed if they are faster processes than the self-focusing and thus prevent it. These competing processes will be investigated in future work. But in the present case we are considering steady state self-focusing of KAWs, which is valid when the observational time ( $T_{\text{obs}}$ ) is of the order of or greater than the ponderomotive nonlinearity setting time ( $\tau_d$ ). In the present case, the ponderomotive nonlinearity setting time ( $\tau_d$ ) comes out to be 114 seconds. For the value of  $k_x = 1/r_0$  and by setting appropriate decay wave frequencies and wave numbers, the decay instability growth time ( $T_{\text{dnl}}$ ) may be greater than, less than, or equal to  $\tau_d$ , depending upon the decay wave numbers.

[39] **Acknowledgments.** This work is partially supported by DST (India) and ISRO (India) under RESPOND program. One of the authors (N.K.D.) is grateful for valuable conversations with H. D. Pandey, Karuna Batra and H. D. Singh.

[40] Philippa Browning thanks the reviewers for their assistance in evaluating this paper.

## References

- Akhmanov, S. A., A. P. Sukhorukov, and R. V. Khokhlov (1968), Self-focusing and diffraction of light in a nonlinear medium, *Sov. Phys. Uspekhi*, **10**, 609–636.
- Belcher, J. W., and L. Davis Jr. (1971), Large-amplitude Alfvén waves in the interplanetary medium, *J. Geophys. Res.*, **76**(16), 3534–3563, doi:10.1029/JA076i016p03534.
- Bellan, P. M., and K. Stasiewicz (1998), Fine-scale cavitation of ionospheric plasma caused by inertial Alfvén wave ponderomotive force, *Phys. Rev. Lett.*, **80**, 3523–3526.
- Chaston, C. C., J. R. Johnson, M. Wilber, M. Acuna, M. L. Goldstein, and H. Reme (2009), Kinetic Alfvén wave turbulence and transport through a reconnection diffusion region, *Phys. Rev. Lett.*, **102**, 015001.
- Chen, L., Z. Lin, and R. White (2001), On resonant heating below the cyclotron frequency, *Phys. Plasmas*, **8**, 4713–4716.
- Cho, J., and A. Lazarian (2004), The anisotropy of electron magnetohydrodynamic turbulence, *Astrophys. J.*, **615**, L41–L44.
- Cho, J., and A. Lazarian (2009), Simulations of electron magnetohydrodynamics turbulence, *Astrophys. J.*, (EP), **701**, 236, doi:10.1088/0004-637X/701/1/236.
- Coleman, P. J., Jr. (1966), Hydromagnetic waves in the interplanetary plasma, *Phys. Rev. Lett.*, **17**, 207–211.
- Cranmer, S. R., G. B. Field, and J. L. Kohl (1999), Spectroscopic constraints on models of ion cyclotron resonance heating in the polar solar corona and high-speed solar wind, *Astrophys. J.*, **518**, 937–947.
- Eastwood, J. P., T. D. Phan, S. D. Bale, and A. Tjulin (2009), Observations of turbulence generated by magnetic reconnection, *Phys. Rev. Lett.*, **102**, 035001.
- Gary, S. P., S. Saito, and H. Li (2008), Cascade of whistler turbulence: Particle-in-cell simulations, *Geophys. Res. Lett.*, **35**, L02104, doi:10.1029/2007GL032327.
- Goertz, C. K., and R. W. Boswell (1979), Magnetosphere-ionosphere coupling, *J. Geophys. Res.*, **84**(A12), 7239–7246, doi:10.1029/JA084iA12p07239.
- Goldstein, M. L., D. A. Roberts, A. E. Deane, S. Ghosh, and H. K. Wong (1999), Numerical simulation of Alfvénic turbulence in the solar wind, *J. Geophys. Res.*, **104**(A7), 14,437–14,451, doi:10.1029/1998JA900128.
- Ji, H., S. Terry, M. Yamada, R. Kulsrud, A. Kuritsyn, and Y. Ren (2004), Electromagnetic fluctuations during fast reconnection in laboratory plasma, *Phys. Rev. Lett.*, **92**, 115001.
- Kennel, C. F., and F. Engelmann (1966), Velocity space diffusion from weak plasma turbulence in a magnetic field, *Phys. Fluids*, **9**, 2377–2388.
- Larsson, J., and L. Stenflo (1975), On the nonlinear interaction between whistler and Alfvén waves, *J. Geophys. Res.*, **80**, 2325–2326, doi:10.1029/JA080i016p02325.
- Leamon, R. J., C. Smith, N. Ness, and H. Wong (1999), Dissipation range dynamics: Kinetic Alfvén wave and the importance of  $b_{\text{ex}}$ , *J. Geophys. Res.*, **104**(A10), 22,331–22,344, doi:10.1029/1999JA900158.
- Leamon, R. J., W. H. Mathaeus, C. W. Smith, G. P. Zank, and D. J. Mullan (2000), MHD-Driven kinetic dissipation in the solar wind and corona, *Astrophys. J.*, **537**, 1054–1062.
- Norqvist, P., M. André, L. Eliason, A. L. Eriksson, L. Blomberg, H. Lühr, and J. L. Clemmons (1996), Ion cyclotron heating in the dayside magnetosphere, *J. Geophys. Res.*, **101**, 13,179–13,193, doi:10.1029/95JA03596.
- Onishchenko, O. G., O. A. Pokotolov, R. Z. Sagdeev, L. Stenflo, R. A. Treumann, and M. Balikhin (2004), Generation of convective cells by kinetic Alfvén waves in the upper ionosphere, *J. Geophys. Res.*, **109**, A03306, doi:10.1029/2003JA010248.
- Rogers, B. N., R. E. Denton, J. F. Drake, and M. A. Shay (2001), Role of dispersive waves in collisionless magnetic reconnection, *Phys. Rev. Lett.*, **87**, 195004.
- Sahraoui, F., et al. (2003), ULF wave identification in the magnetosheath: The k-filtering technique applied to Cluster II data, *J. Geophys. Res.*, **108**(A9), 1335, doi:10.1029/2002JA009587.
- Sahraoui, F., M. L. Goldstein, P. Robert, and Y. V. Khotyaintsev (2009), Evidence of a cascade and dissipation of solar-wind turbulence at the electron gyroscale, *Phys. Rev. Lett.*, **102**, 231102.
- Schekochihin, A. A., S. C. Cowley, W. Dorland, G. W. Hammett, G. G. Howes, E. Quataert, and T. Tatsuno (2009), Astrophysical gyrokinetics: Kinetic and fluid turbulent cascades in magnetized weakly collisional plasmas, *Astrophys. J. Supp.*, **182**, 310–377.
- Shukla, A., and R. P. Sharma (2002), Nonlinear kinetic Alfvén waves associated with saturating nonlinearity: application to solar wind and coronal heating, *J. Atmos. Sol. Terr. Phys.*, **64**, 661–668.
- Shukla, P. K., and L. Stenflo (1999), Plasma density cavitation due to inertial Alfvén wave heating, *Phys. Plasmas*, **6**, 4120–4122.
- Shukla, P. K., and L. Stenflo (2000), Generation of localized density perturbations by shear Alfvén waves, *Phys. Plasmas*, **7**, 2738–2739.
- Shukla, P. K., L. Stenflo, and R. Bingham (1999), Nonlinear propagation of inertial Alfvén waves in auroral plasmas, *Phys. Plasmas*, **6**, 1677–1680.
- Stasiewicz, K., Y. Khotyaintsev, M. Berthomier, and J. E. Wahlund (2000a), Identification of widespread turbulence of dispersive Alfvén waves, *Geophys. Res. Lett.*, **27**(2), 173–176, doi:10.1029/1999GL010696.
- Stasiewicz, K., et al. (2000b), Small scale Alfvénic structure in the aurora, *Space Sci. Rev.*, **92**, 423–533.
- Stawicki, O., S. P. Gary, and H. Li (2001), Solar wind magnetic fluctuation spectra: Dispersion versus damping, *J. Geophys. Res.*, **106**(A5), 8273–8281, doi:10.1029/2000JA000446.
- Stefant, J. R. (1970), Alfvén wave damping from finite gyroradius coupling to the ion acoustic mode, *Phys. Fluids*, **13**, 440–450.
- Unti, J. W., and N. Neugebauer (1968), Alfvén waves in solar wind, *Phys. Fluids*, **11**, 563–568.
- Voitenko, Yu. M. (1998), Three-wave coupling and parametric decay of kinetic Alfvén waves, *J. Plasma Phys.*, **60**, 497–514.
- Wygant, J. R., et al. (2002), Evidence for kinetic Alfvén waves and parallel electron energization at 4–6  $R_E$  altitudes in the plasma sheet boundary layer, *J. Geophys. Res.*, **107**(A8), 1201, doi:10.1029/2001JA900113.
- Yukhimuk, V., R. R. Dupre, and E. Symbalisty (1999), Geomagnetic pulsation generation as a result of whistler wave scattering, *Phys. Plasmas*, **6**, 264–267.
- P. K. Chauhan, Grupo de Laser e Plasmas, Instituto Superior Técnico, Av. Rovisco Pais, P-1049001 Lisbon, Portugal.
- N. K. Dwivedi and R. P. Sharma, Centre for Energy Studies, Indian Institute of Technology, Delhi 110016, India. (navin.dwivedi@gmail.com)
- M. L. Goldstein, NASA Goddard Space Flight Center, Code 673, Greenbelt, MD 20771, USA.